Magnetic phase transition in single crystals of the chiral helimagnet $Cr_{1/3}NbS_2$

N. J. Ghimire,[1,2] M. A. McGuire,[2] D. S. Parker,[2] B. Sipos,[2] S. Tang,[2] J.-Q. Yan,[2,3] B. C. Sales,[2] and D. Mandrus[1,2,3]

[1]*Department of Physics and Astronomy, The University of Tennessee, Knoxville, Tennessee 37996, USA*

[2]*Materials Science and Technology Division, Oak Ridge National Laboratory, Oak Ridge, Tennessee 37831, USA*

[3]*Department of Materials Science and Engineering, The University of Tennessee, Knoxville, Tennessee 37996, USA*

(Received 13 September 2012; published 11 March 2013)

The chiral helimagnet $Cr_{1/3}NbS_2$ has been investigated by magnetic, transport, and thermal properties measurements on single crystals and by first-principles electronic structure calculations. From the measured field and temperature dependence of the magnetization for fields applied perpendicular to the *c* axis, the magnetic phase diagram has been constructed in the vicinity of the phase transition. A transition from a paramagnetic to a magnetically ordered phase occurs near 120 K. The transition is found to strongly affect the electrical transport. The resistivity decreases sharply upon cooling near 120 K, and the spin reorientation from the helimagnetic ground state to the commensurate ferromagnetic state is evident in the magnetoresistance. At high fields, a large magnetoresistance (55% at 140 kOe) is observed near the magnetic transition temperature. Heat capacity and electronic structure calculations show that the density of states at the Fermi level is low in the magnetically ordered state.

DOI: 10.1103/PhysRevB.87.104403 PACS number(s): 75.30.Kz, 75.10.−b

I. INTRODUCTION

Complex magnetic textures have recently been observed in some magnetic materials crystallizing in the cubic space group $P2_13$. MnSi,[1] $Fe_{1-x}Co_xSi$ ($0.2 \leqslant x \leqslant 0.5$),[3,4] FeGe,[2] and Cu_2OSeO_3[5] are those materials where the ground-state magnetic structure is found to have a modulated helimagnetic arrangement of spins incommensurate with the underlying crystal lattice. In addition to this, another remarkable similarity in these materials is that in a certain range of magnetic fields and at temperatures just below the transition temperature, a distinct skyrmion lattice phase exists. A skyrmion is a magnetic vortex, a structure reminiscent of the Abrikosov vortices in type-II superconductors.[6–9] It is to be noted that these similarities have been observed irrespective of the nature of the electrical conductivity of the materials. MnSi[10] and FeGe[11] are metals, $Fe_{1-x}Co_xSi$ ($0.2 \leqslant x \leqslant 0.5$)[12] shows a complex metallic behavior with negative temperature coefficient in the lower temperature ($\leqslant$50 K) helical state, and Cu_2OSeO_3[5] is an insulator. External magnetic field is found to destabilize the ground-state helical ordering with an eventual transition to commensurate ferromagnetic states in the first three materials and a ferrimagnetic state in the last one. All these materials belong to the same space group $P2_13$, which lacks an inversion center. The ground state chiral helimagnetic ordering in the noncentrosymmetric space group has been well understood to be due to the competition between the symmetric exchange interaction that favors a parallel arrangement of spins and the antisymmetric Dzyaloshinsky-Moriya (DM) interaction that favors a perpendicular arrangement of spins, which results in a modulated helimagnetic spin structure.[13–16] The origin of the skyrmion phase, however, is still unclear on a general level. Theoretically, it has been predicted to occur in a wide range of noncentrosymmetric magnets.[6,17,18] However, experimentally, it has been observed in materials belonging to only one space group. At the same time, recent studies have shown that the noncentrosymmetric magnets provide a platform for the observation of a magnetic blue phase, a novel magnetic state, formed by the twisting of the chiral helices, reminiscent of the blue phase observed in nematic liquid crystals.[19–21]

$Cr_{1/3}NbS_2$ is a material that bears the common properties of the materials mentioned above but has a different crystallographic symmetry. It crystallizes in a noncentrosymmetric hexagonal space group $P6_322$ belonging to the point group D_6^6,[22] one of the symmetry groups in which ferromagnets have been theoretically predicted to have a skyrmion lattice.[18] It orders magnetically into a helimagnetic ground state with a period of about 480 Å below about 116–127 K and is known to have metallic behavior below room temperature.[23–26] The spins are arranged ferromagnetically in the *ab* plane and the helix is along the *c* axis. The effect of magnetic field in the *ab* plane has been found to be dramatic with a metamagnetic transition observed at an applied field near 1200–1500 Oe.[24] A nonlinear periodic magnetic state called a soliton lattice was predicted for this material[27,28] and recently observed in a thin specimen studied with small angle electron diffraction and Lorentz force microscopy.[29] A magnetic field applied perpendicular to the direction of the helix destabilizes the helical structure gradually into a soliton lattice with an eventual incommensurate-to-commensurate transition into a ferromagnetic state at the critical field of 2300 Oe. Manipulation of the spin spiral with magnetic field has generated interest in this material for spintronics applications.[30–33]

The first helimagnetic ground state in this material was experimentally observed by Miyadai *et al.*[24] by means of small angle neutron scattering conducted on a powder sample, which was in accordance with the prediction of the helimagnetic structure by Moriya and Miyadai[34] based on the magnetic measurements and the subsequent theoretical interpretation in terms of the DM interaction in a noncentrosymmetric magnet. In earlier studies, Parkin *et al.*[25,26] found it to order ferromagnetically below 120 K with the basal plane being the easy axis.

In this paper, we present experimental results obtained on single crystals of $Cr_{1/3}NbS_2$ together with results from

electronic structure calculations. The temperature dependence of dc susceptibility and the magnetization curves is reported both parallel and perpendicular to the c axis. The temperature dependence of electrical resistivity, specific heat capacity, thermal conductivity, and Seebeck coefficient in zero magnetic field and their behavior in magnetic fields applied perpendicular to the c axis are investigated. Results of band structure and density of states (DOS) calculations are presented both in the nonmagnetic and magnetic states.

II. CRYSTAL CHEMISTRY

$Cr_{1/3}NbS_2$ crystallizes in the Nb_3CoS_6, hp20 structure type.[23] It forms a hexagonal layered structure, as depicted in Fig. 1(a), containing 20 atoms per unit cell. Twelve sulfur atoms occupy the general site. There are six niobium atoms in two inequivalent positions: 4f and 2a. The Cr atoms are intercalated in the octahedral holes (2c sites) between the trigonal prismatic layers of 2H-NbS_2. The unit cell parameters obtained from the x-ray data collected from the powdered crystals are $a = 5.741$ Å and $c = 12.101$ Å, which are in good agreement with the reported values.[23,24] The Cr-Cr distance is closest within the layer in the ab plane (5.741 Å). Along the c axis, the nearest Cr-Cr distance is 6.847 Å. $Cr_{1/3}NbS_2$ belongs to a large family of layered materials that are formed by intercalation of transition metal elements within the layers of the first row transition metal dichalcogenides. The structure depends on the amount of intercalation in the layer. In the absence of intercalated atoms, the host transition metal dichalcogenide layers are coupled through weak van der Waals bonds. The intercalation of a transition metal strengthens the bonding with the possibility of charge transfer from the intercalated atoms to the transition metal atoms in the layer, which brings about strong changes in the electronic structure and corresponding changes in the electrical transport and magnetic properties.[35]

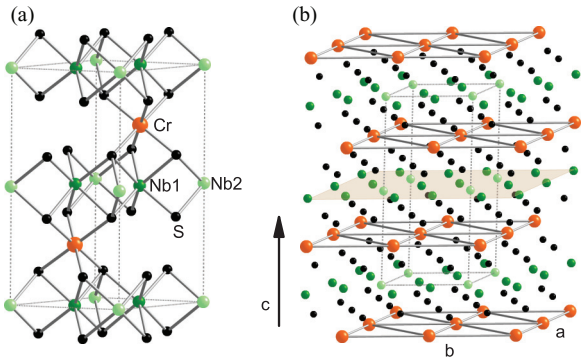

FIG. 1. (Color online) (a) Hexagonal crystal structure of $Cr_{1/3}NbS_2$. The intercalated chromium atoms occupy the octahedral interstitial holes between the trigonal prismatic layers of 2H-NbS_2. (b) Structure of $Cr_{1/3}NbS_2$ emphasizing the layers of Cr atoms in the ab plane. The Cr-Cr distance is shortest in the plane. The dotted lines show the unit cell. The biggest (orange) balls represent Cr atoms, the medium (green) balls represent Nb atoms, and the smallest (black) balls represent S atoms. Nb atoms are in two inequivalent sites labeled as Nb1 and Nb2.

III. EXPERIMENTAL DETAILS

Crystals of $Cr_{1/3}NbS_2$ were grown by chemical vapor transport using iodine as the transport agent.[24] Single crystals of various sizes with dimensions as large as 8 mm × 7 mm × 1 mm were obtained. X-ray diffraction from powdered crystals confirmed the $P6_322$ structure and revealed no impurity phases. Energy dispersive x-ray spectroscopy (EDS) results along with the magnetic transition temperature clearly distinguish these crystals to be $Cr_{1/3}NbS_2$.[25,36] No iodine was detected in the crystals by the EDS measurements. Magnetic properties were measured using a Quantum Design Magnetic Property Measurement System (MPMS) adopting a field cooling approach. Resistivity, magnetoresistance, thermal conductivity, and Seebeck coefficient were all measured in a Quantum Design Physical Property Measurement System (PPMS). A four wire configuration with platinum wires and Epotek H20E silver epoxy were used for the resistivity and magnetoresistance measurements.

IV. RESULTS AND DISCUSSION

A. Magnetic properties

Figure 2 shows M/H as a function of temperature with the applied magnetic field perpendicular [see Fig. 2(a)] and parallel [see Fig. 2(b)] to the c axis. With the magnetic field applied perpendicular to the c axis, at the lower field (1 kOe), a small kink is observed at about 117 K. This kink is not observed at 10 kOe. No such kink is observed in M/H versus T when the magnetic field is applied parallel to the c axis. These results are consistent with previous measurements by Miyadai *et al.*[24] As

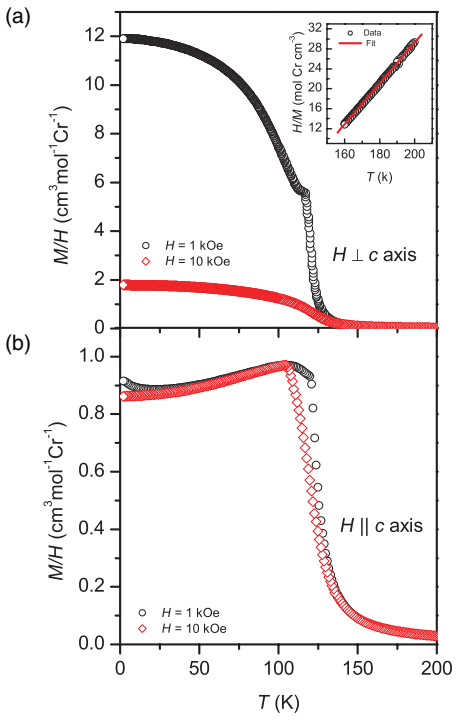

FIG. 2. (Color online) M/H as a function of temperature at the fields indicated with the magnetic field applied (a) perpendicular to the c axis and (b) parallel to the c axis. Inset in (a) shows the fit to the Curie-Weiss law for the data taken at 1 kOe above 160 K.

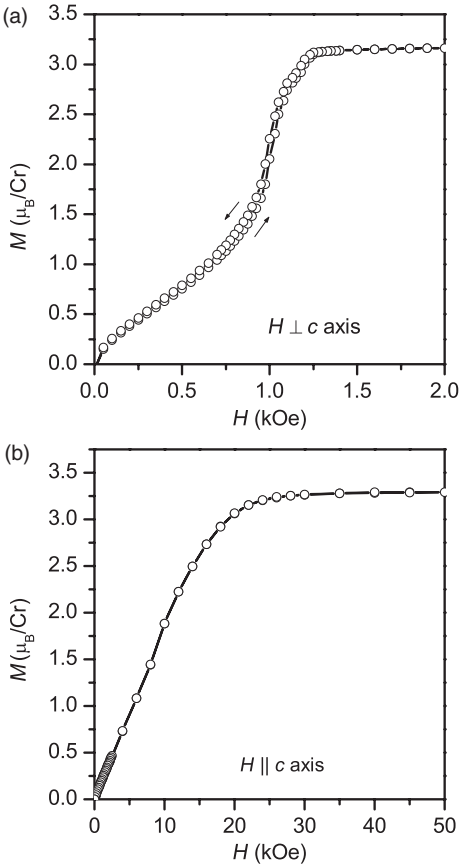

FIG. 3. M vs H measured at a temperature of 2 K with the magnetic field applied (a) perpendicular, and (b) parallel to the c axis. Note the different scales on the x axis.

the material is known to have helimagnetic ordering in lower fields with the helix directed along the c axis,[29] the kink may represent the onset of the helical state. Such a kink has also been observed in other known helimagnets such as MnSi,[37] FeGe,[38] and $Fe_{1-x}Co_xSi$.[12] $Cr_{1/3}NbS_2$ follows Curie-Weiss behavior at higher temperatures. The inset in Fig. 2(a) shows the Curie-Weiss fit of $\chi = \frac{C}{T-\theta_{cw}}$ to the high temperature part of data measured with an applied field of 1 kOe. The parameters obtained are the Curie constant $C = 2.4$ K cm^3 mol $^{-1}$ Cr^{-1} and the Curie-Weiss temperature $\theta_{CW} = 127$ K. The effective moment per mole of chromium atoms, p_{eff}, calculated from the Curie constant is 4.4 μ_B, which is consistent with the values reported by Parkin *et al.*[36] (4.3 μ_B and 4.1 μ_B for field applied parallel and perpendicular to the c axis, respectively).

The anisotropic nature of the low-temperature magnetism in $Cr_{1/3}NbS_2$ is evident in Fig. 3. Applying a field along the c axis [see Fig. 3(b)] simply rotates the ordered moments out of the ab plane. This results in a nearly linear increase in M with H up to $H = 20$ kOe. When the field is applied in the ab plane [see Fig. 3(a)], more complex behavior is observed, which will be addressed further in the following discussion. The moment saturates to the same value of about 3.2 μ_B/Cr, close to the expected value of 3 for $S = 3/2$, in both orientations. But this occurs at a much lower field when H is applied in the ab plane, indicating a strong preference for the moments to remain perpendicular to the c axis.

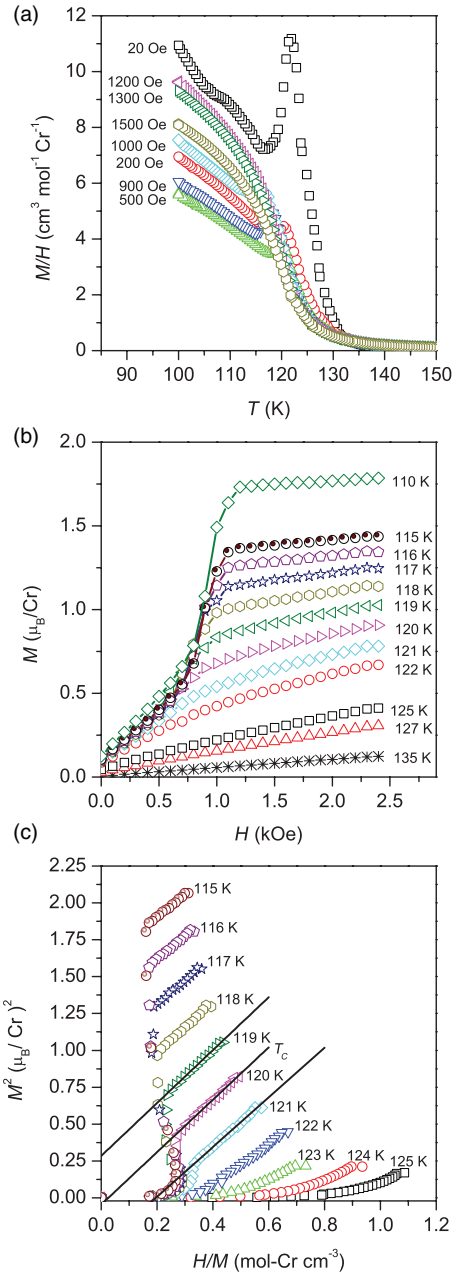

FIG. 4. (Color online) Magnetic properties of $Cr_{1/3}NbS_2$ near the transition temperature in low magnetic field applied perpendicular to the c axis. (a) M/H as a function of temperature at indicated fields. (b) M vs H at selected temperatures, and (c) Arrott plots. The solid lines are the extrapolation of the M^2 vs H/M data at higher fields.

Figure 4 shows various magnetic properties near the magnetic ordering temperature with the magnetic field applied perpendicular to the c axis, i.e., perpendicular to the helical axis. M/H as a function of temperature at the indicated magnetic fields are depicted in Fig. 4(a). The kink due to the onset of helimagnetic ordering is not observed for $H \geqslant 1200$ Oe. At 119 K, M versus H [see Fig. 4(b)] increases linearly at low field. At around 500 Oe, it shows a change in slope. Another slope change is observed around 1000 Oe. The region between 500–1000 Oe shows a steeper slope. With the decrease in temperature, the lower end of the steeper slope

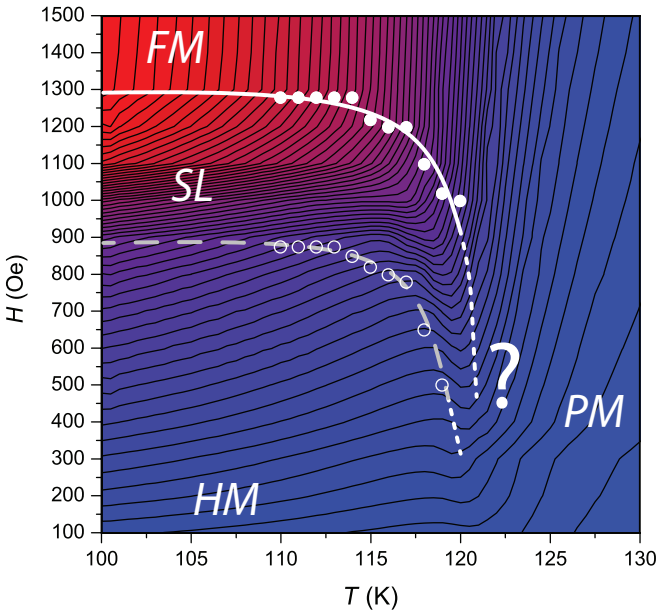

FIG. 5. (Color online) Contours of $M(H,T)$ determined from M vs T measurements at fields from 100 to 1500 Oe applied in the ab plane. The white data points were determined from M versus H measurements at temperatures from 110 to 120 K. The question mark "?" represents the region of transition from a paramagnetic (PM) to a helimagnetic (HM) phase. The details of this phase evolution have not yet been determined.

moves towards higher field and a sharp change is observed around 1000 Oe. The moments saturate above about 1300 Oe. This behavior is not observed at higher temperatures. A contour plot of M versus H and T near the phase transition region is shown in Fig. 5. This provides a useful visualization of the magnetic phase diagram for $Cr_{1/3}NbS_2$. The magnetization values are highest in the red area (upper left) and lowest in the blue areas. The solid white line is a guide to the eye, and follows the temperature and field dependence of the ferromagnetic transition (white circles) determined from the measured saturation field at a fixed temperature [see, for example, the 110 K curve in Fig. 4(b)]. These points separate the soliton lattice (SL) phase from the ferromagnetic (FM) phase. The details of how the complex helimagnetic (HM) and SL phases evolve upon cooling from the paramagnetic (PM) phase have not been determined. Here, we observed the transition from the soliton phase to the ferromagnetic state at a field of about 1300 Oe for temperatures below about 117 K. A phenomenological description explains the evolution of the soliton lattice under an external magnetic field.[39–41] Over a certain range of the magnetic field applied perpendicular to the helical axis, the helimagnetic ground state gets distorted slowly into an inhomogeneous helicoid, however, the period does not change significantly. With further increase in the applied field, there appears a sharp crossover when the 360° turns become discernible as solitonic kinks. But they are still bound and there is no real phase transition. It is a nonlinear crossover behavior within the same modulated phase. The lower set of points (open circles) in the phase diagram (see Fig. 5) represent these states at different fields and temperatures. On further increasing the applied field, the core of the kinks remain almost stable in shape, but their tails rapidly increase to resemble domains with magnetization in the field direction. This is the range of rapidly increasing magnetization between the lower and the upper set of points in the phase diagram. The magnetic phase transition from soliton lattice to the ferromagnetic state (or the free soliton state) is reached when the solitons become unbound. During this process, in reality, not all the solitons are pushed out of a finite crystal, rather they can be preserved as a gas of free solitons or remain somewhere pinned at defects in the crystal.[42] Therefore, depending on the maximum field value reached above this transition, cycling the field up and down through such a nucleation transition may eventually show a hysteresis, as remaining solitons may or may not enter back into the crystal and bind together to form a lattice again. This explains the observed hysteresis in the M versus H measurements as observed in Fig. 3(a) which, otherwise usually represents a discontinuous phase transition. But, the heat capacity measurements (see Fig. 9) show a second-order phase transition in all range of magnetic fields measured. However, this SL-FM transition is apparent in the thermal and transport properties discussed below.

Figure 4(c) shows variation of $M^2(H,T)$ as a function of $H/M(H,T)$ at different temperatures in the region of the magnetic transition. These Arrott plots in the ferromagnetic state (at higher fields) are linear. The isothermal line in the Arrott plot passing through the origin represents the transition temperature.[43] Thus the Curie temperature (T_C) for $Cr_{1/3}NbS_2$ is taken to be 120 K.

B. Transport properties

Electrical resistivity as a function of temperature is depicted in Fig. 6(a). Interestingly, there is an abrupt and large change of the resistivity in the vicinity of the magnetic transition temperature. Above T_C, up to the measured temperature of 300 K, there is a slight decrease in the resistivity with temperature. It contrasts with the behavior of conventional metallic ferromagnets where there is a decrease in the resistivity on cooling over the entire temperature range and a change in slope or a kink near the magnetic transition temperature due to reduction in the spin disorder scattering. Hall effect measurements at 200 K with the current in the ab plane and the magnetic field along the c axis gave a Hall coefficient of 2×10^{-2} cm^3 C^{-1} at 200 K (for a single band, this would correspond to 10^{20} holes cm^{-3}). This along with the measured resistivity values near 2 mΩ cm above the transition, suggests the material may be described as low carrier concentration metal or heavily doped semiconductor. The decrease in ρ with increasing temperature at the highest temperatures investigated indicates that this is not a simple metal in the paramagnetic state. Similar high temperature behavior has been observed in some metallic, uranium-based, ternary compounds UPt_2Si_2,[44] UPd_2Si_2,[45] and URh_2Si_2.[46] Comparison of the transport properties with those reported in Ref. 25 shows that the crystals studied here have higher resistivity and higher Hall coefficients than those previously studied. Figure 6(b) shows the temperature dependence of the resistivity at various magnetic fields up to 140 kOe. As expected the effect of the magnetic field is strongest near the magnetic transition temperature. The sharp change observed

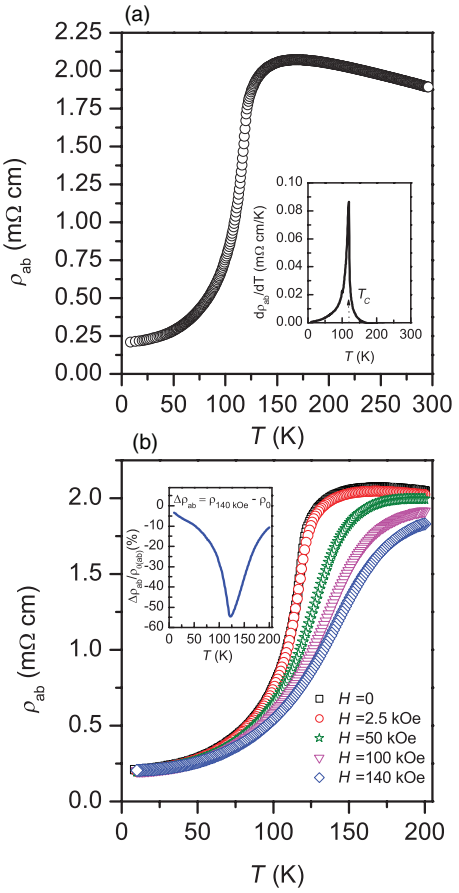

FIG. 6. (Color online) (a) Electrical resistivity of $Cr_{1/3}NbS_2$ as a function of temperature measured in the *ab* plane. Inset shows the temperature derivative of the resistivity. (b) Temperature dependence of electrical resistivity of $Cr_{1/3}NbS_2$ measured in the *ab* plane at indicated magnetic fields applied parallel to the plane. Inset shows the magnetoresistance where $\Delta\rho_{ab} = \rho_{140kOe} - \rho_0$.

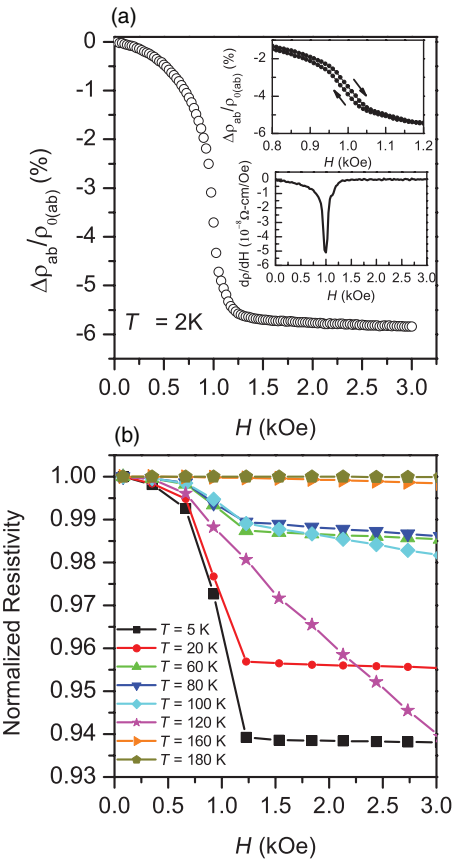

FIG. 7. (Color online) Low-field magnetoresistance of $Cr_{1/3}NbS_2$ measured in the *ab*-plane with magnetic field applied parallel to the plane. (a) Magnetoresistance measured at $T = 2$ K. The upper inset shows the change in slope in the magnetoresistance in the vicinity of the field where the metamagnetic transition is observed in the magnetization measurements. The lower inset shows the derivative of the resistivity with respect of the field. It shows that the sharp change occurs at 1 kOe. (b) Normalized resistivity measured in the *ab* plane as a function of magnetic field applied parallel to the plane at indicated temperatures.

at lower fields near T_C are skewed to higher temperatures by magnetic field, as may be expected for a ferromagnet. However, a strong suppression of the resistivity upon cooling is still seen at 140 kOe. The inset of Fig. 6(b) shows the magnetoresistance obtained by subtracting the resistivity measured at zero applied magnetic field from the resistivity measured at the magnetic field of 140 kOe. A very large magnetoresistance of about 55% is observed at the Curie temperature.

Figure 7(a) shows the magnetoresistance measured at 2 K up to an applied magnetic field of 3 kOe. It shows a maximum magnetoresistance of about 5.5%. The change in magnetoresistance around 1 kOe is quite sharp and coincides with the SL phase indicated by magnetization measurements. At 2 K, a small hysteresis is observed [upper inset in the Fig. 7(a)] and it appears in the same region where hysteresis is seen in the magnetization measurements [see Fig. 2(a)]. The hysteresis persists up to 100 K (not shown). The lower inset shows the derivative of the resistivity with respect to the applied magnetic field, which clearly shows the sharp change occurring at the applied field of 1 kOe. This behavior in the resistivity also seems consistent with the soliton model. As discussed above, as the applied magnetic field starts aligning the moments towards its direction, spin disorder scattering decreases thereby reducing the electrical resistivity. As the magnetic field causes the transition from the soliton phase to the ferromagnetic state, all the moments are aligned in the direction of the field and thus no further change is seen in the resistivity at higher fields. The low-field magnetoresistance behavior is found to be qualitatively similar at all temperatures measured below 100 K. Figure 7(b) shows the normalized resistivity defined by $\rho_H/\rho_{H=0}$ as a function of magnetic field. Above 120 K, the resistivity varies little with field, while below 120 K, the resistivity behavior is similar to that observed at 2 K [cf. Fig. 7(a)]. Interestingly, at $T_C = 120$ K $\rho(H)$ has a strong field dependence but, unlike at lower temperatures, it does not saturate near 1 kOe. The origin of this behavior is unclear, and highlights the lack of detailed understanding of the complex behavior of helimagnetic materials near their critical temperatures.

The temperature-dependent thermal conductivity κ(T) of $Cr_{1/3}NbS_2$ is shown in Fig. 8(a). Upon heating, κ increases up to about 65 K above which it decreases slightly up to 200 K.

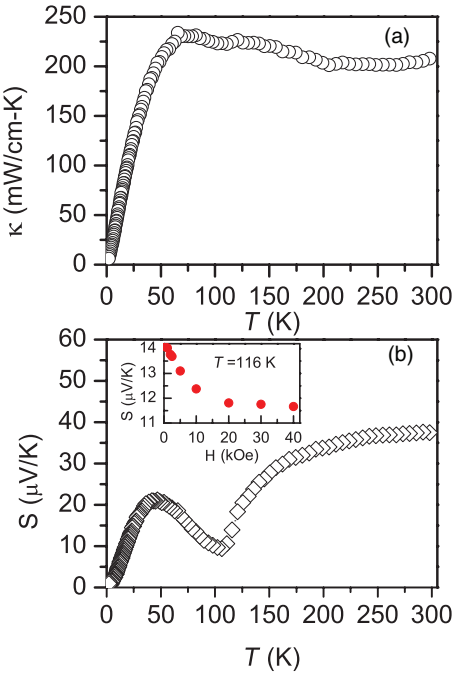

FIG. 8. (Color online) (a) Temperature dependence of thermal conductivity measured in the *ab* plane and (b) temperature dependence of Seebeck coefficient measured in the *ab* plane. Inset shows the magnetic field dependence of the Seebeck coefficient at $T = 116$ K with magnetic field applied parallel to the *ab* plane.

In general, the thermal conductivity of a metal is the sum of electronic and lattice terms. The electronic contribution to the thermal conductivity can be estimated by the Wiedemann-Franz law:[47] $\kappa_e \rho / T = L$, where κ_e is the electronic part of the thermal conductivity, ρ is the electrical resistivity, and $L = 2.45 \times 10^{-8}$ WΩK^{-2} is the Lorenz number. The maximum value of κ_e estimated from Wiedemann-Franz law occurs around 65 K and is less than 5 mW/cm K. This indicates that the thermal conductivity is mainly due to phonons.

Figure 8(b) shows the temperature dependence of the Seebeck coefficient (S). At all temperatures measured, the Seebeck coefficient is positive. However, it shows a remarkable minimum slightly below the magnetic transition temperature. The Hall coefficient of $Cr_{1/3}NbS_2$[25] is reported to be positive above 180 K and below 20 K, and negative between these temperatures, with a sharp minimum at 115 K. This coincides with the region of minimum observed in S in Fig. 8(b). $Cr_{1/3}NbS_2$ is metallic with multiple bands contributing to the Fermi surface (see Sec. IV D). This complicates the interpretation of Hall and Seebeck coefficient data. In the simplest interpretation, the Hall data suggest electron dominated transport between 20 and 180 K, and primarily hole conduction at higher and lower temperatures. The Seebeck coefficient is positive over this entire temperature range, but the observed minimum is consistent with increased electron contribution peaking near 115 K. The data may indicate multiple bands near the Fermi energy with contributions to the transport properties, which vary with temperature due to changes in band energies with temperature, or the probing of bands further from the Fermi energy at higher temperatures. In addition to changes in the electronic structure, changes in charge carrier scattering and mobilities may be associated with the magnetic ordering in $Cr_{1/3}NbS_2$. This could also contribute to the temperature dependence of the Hall and Seebeck coefficients near the transition temperature. Interestingly, the resistivity and Seebeck coefficients shown in Figs. 6 and 8 show some similarity to the reported behavior of LaFeAsO,[48] $BaFe_2As_2$,[49] and related materials near their structural/magnetic phase transitions. The Seebeck coefficient is found to have a magnetic field dependence at 116 K. With the external magnetic field applied perpendicular to the c axis, S decreases up to about 20 kOe, above which it remains constant [see Fig. 8(b)], which suggests either a spin-entropy contribution to S, a strong influence of H on the band structure, or the effects of the magnetic field on the scattering of carriers.

C. Heat capacity

The temperature dependence of specific heat shows clear lambda anomaly in the vicinity of the magnetic ordering temperature at ambient field as shown in Fig. 9(a). The magnetic field dependence of the heat capacity anomaly is depicted in [see Fig. 9(b)]. The lambda peak does not change significantly up to 800 Oe. However, it is found to decrease clearly at a field of 1500 Oe. The peak is suppressed

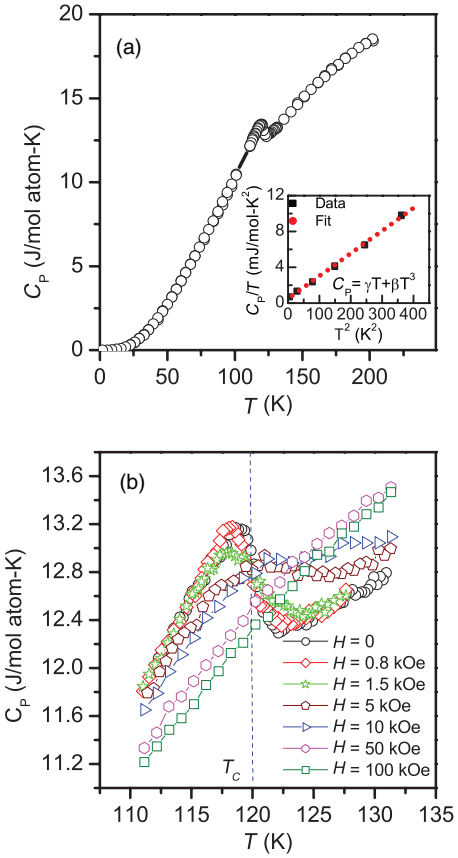

FIG. 9. (Color online) (a) Heat capacity of $Cr_{1/3}NbS_2$ as a function of temperature at zero applied magnetic field. (b) Temperature dependence of the specific heat near the magnetic transition temperature measured at indicated magnetic fields applied perpendicular to the c axis.

with the further increase in the magnetic field and is not observed above 50 kOe. Application of a magnetic field increased the heat capacity above the magnetic transition temperature (120 K) and suppressed the heat capacity below it. A decrease in the λ peak is found to occur in the ferromagnetic state when the moments are aligned in the direction of the magnetic field. This behavior is consistent with the results obtained in the magnetization and magnetoresistance measurements.

The low-temperature specific heat can be modeled well with electronic and phononic contributions. The inset of Fig. 9(a) shows a fit to $C/T = \gamma + \beta T^2$, where γ is the Sommerfeld coefficient and β is the phononic heat capacity coefficient. The fit yielded $\gamma = 0.40 \pm 0.25$ mJ mol^{-1} K^{-2} and $\beta = 0.0263 \pm 0.0047$ mJ mol^{-1} K^{-4}. The electron density of states at the Fermi energy (E_F) and the Debye temperature (T_D) can be estimated from γ and β using the relations $N(E_F) = 3\gamma/\pi^2 k_B^2$ and $T_D = (5\beta/12R\pi^4)^{-1/3}$, respectively, where k_B is the Boltzmann constant and R is the universal gas constant. The calculated values are $N(E_F) = 3.40$ states (eV u.c.)$^{-1}$ and $T_D = 419$ K. The experimentally determined DOS at the Fermi energy is comparable to the value [2.76 states (eV u.c.)$^{-1}$] obtained from the electronic structure calculations in the magnetic state presented below (see Fig. 12).

D. First-principles calculations

In order to understand theoretically the effect of the magnetic ordering, we have performed first-principles density functional theory calculations, using the generalized gradient approximation of Perdew, Burke, and Ernzerhof[50] as implemented in the all electron code WIEN2k.[51] We have used the experimental hexagonal lattice constants and internal parameters; no relaxation was performed. Calculations in both a nonmagnetic and a magnetic spin-polarized state were performed, using 120 k points in the irreducible Brillouin zone and LAPW sphere radii of $2.07a_0$, $2.33a_0$, and $2.34a_0$ for the S, Nb, and Cr atoms, respectively (here, a_0 is the Bohr radius = 0.529177 Å). An $RK_{\max}$ of 7, where R is the minimum atomic sphere radius and K the largest plane-wave vector used in the expansion, was used.

Regarding the spin-polarized calculations, a brief discussion is in order. As reported previous experimental evidences[24,29] that the ground state of $Cr_{1/3}NbS_2$ is a very long wavelength (∼480 Å) spiral with adjacent spins in the spiral very nearly parallel, such a magnetic structure, if one attempted to study it in a "brute-force" computational framework, would result in a calculation involving several hundred atoms and several thousand electrons, which would present a nearly intractable problem for standard first-principles approaches. However, a simple observation allows one to perform a much simpler calculation which should be very close in energy and ground-state properties to the actual ground state. The origin of the DM interaction lies in the spin-orbit interaction.[52,53] The energy scale of the relativistic term believed to be responsible for the spiral state is much weaker (a quantitative estimate suggests between one and two orders of magnitude smaller) than the ordinary ferromagnetic Heisenberg nearest-neighbor exchange energy. Thus it is highly likely that the actual energies and properties, such as the density of states of the real

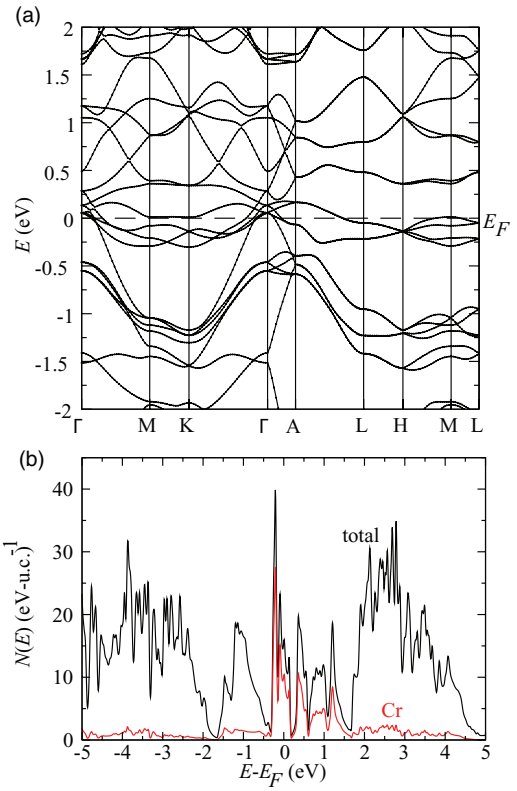

FIG. 10. (Color online) (a) The calculated band structure and (b) density of states of $Cr_{1/3}NbS_2$ in the nonmagnetic state. Note the many Fermi level crossings and corresponding high density of states at E_F.

spiral magnetic ground state, can be described as very nearly those of an ordinary spin-polarized ferromagnetic ground state, with the "spin-up" and "spin-down" contributions simply summed. The DM interaction can be treated as a small perturbation to the main ferromagnetic interaction, so that the actual energy eigenvalues of the physical electrons will not be significantly affected by it. It is then an excellent approximation to take a true ground-state physical observable, such as the density of states, as the *sum* of the separate "spin-up" and "spin-down" contributions. Again, a quantitative estimate suggests that the effect of the DM interaction on the Kohn-Sham eigenvalues is less than 10 meV, which is much smaller than all other relevant energy scales and virtually invisible on the plots presented below.

We begin with the calculated nonmagnetic band structure and density of states, presented in Fig. 10 below. There are several bands crossing the Fermi level, and in addition flat bands virtually abutting the Fermi level from M to K and H to M. There is also a fairly complex structure around the Γ point. As might be expected, this band structure leads to a high density of states at the Fermi level, presented in Fig. 10(b). The Fermi level sits near the middle of a region of fairly elevated DOS, with Fermi level DOS of approximately 15 states/eV unit cell and approximately 10 states/eV unit cell chromium. Given the two Cr atoms in the unit cell and the exchange correlation value I of 0.38 eV for Cr,[54] one finds the Stoner criterion $N_0 I > 1$ well satisfied, with $N_0 I$ on a per Cr basis having the value 1.9. The majority, but not entirety, of the

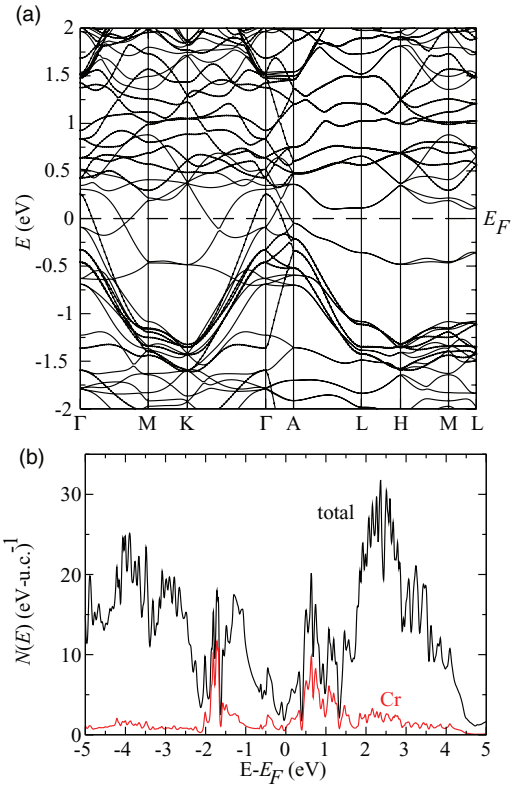

FIG. 11. (Color online) (a) The calculated band structure and (b) density of states of $Cr_{1/3}NbS_2$ in the assumed magnetic state. Most of the Fermi level crossings have disappeared and the density of states shows a substantial pseudogap at E_F.

DOS character near E_F is Cr, suggesting some hybridization of the chemical bonds.

Moving to the magnetic state calculations previously described, we find strong evidence for a magnetic ground state, with the magnetic state some 311 meV per formula unit in energy lower than the nonmagnetic state. In Fig. 11, we present the calculated band structure and density of states for this ground state; as outlined above, we have simply summed the "spin-up" and "spin-down" contributions to the DOS and plotted both band structures on the same plot. The band structure demonstrates far fewer Fermi level crossings,

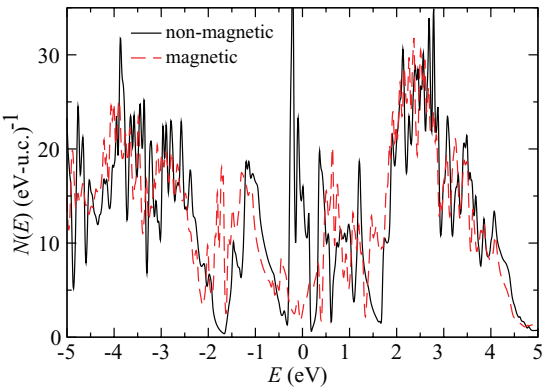

FIG. 12. (Color online) The calculated density of states of $Cr_{1/3}NbS_2$ in the magnetic and nonmagnetic states.

and accordingly examining the density of states we find a substantial loss of spectral weight around E_F. It is instructive to directly compare the magnetic and nonmagnetic DOS, and this is presented in Fig. 12. We note that the significant changes to the DOS are confined to an energy range of ± 2 eV around E_F, despite the large energy gain of nearly an electron-volt per formula unit. The DOS at E_F in the magnetic state is found to be 2.76 states (eV u.c.)$^{-1}$, which is consistent with the experimental value extracted from the low-temperature heat capacity presented above.

V. SUMMARY AND CONCLUSIONS

We have determined the temperature and magnetic field dependence of the magnetic, transport, and thermal properties of $Cr_{1/3}NbS_2$ single crystals. Contours of constant magnetization are utilized to identify key features in the magnetic phase diagram near the transition region (see Fig. 5). The material is magnetically ordered below about 120 K. Below this temperature, increasing the magnetic field applied in the *ab*-plane results in a transition from helimagnetic to ferromagnetic order, with evidence from the previously reported soliton lattice phase at intermediate fields.[29] Evidence for these field- and temperature-induced phase transitions is also seen in resistivity, Seebeck coefficient, and heat capacity results. The resistivity responds strongly to the magnetic ordering, decreasing upon cooling through the magnetic transitions by more than a factor of four. A sharp drop in the Seebeck coefficient is observed upon cooling near 120 K as well. Significant effects of applied magnetic field on these transport properties are also seen in the ordered state, especially near the ordering temperature. Observations include large magnetoresistance (-55% at 140 kOe and 120 K) and $\rho(H)$ data that mimic the $M(H)$ behavior below 120 K, but are anomalous at 120 K. These findings suggest that the magnetic transitions are accompanied by large changes in the electronic structure, which is confirmed by DFT calculations. The calculated DOS in the magnetic state is strongly suppressed relative to the value from nonmagnetic calculations. Since the resistivity decreases upon entering the magnetically ordered state, changes in magnetic scattering of charge carriers are also likely to be important in determining the transport behavior. The large change in the resistivity suggests strong scattering by spin fluctuations above 120 K. Analysis of the heat capacity results indicate a small Sommerfeld coefficient of 0.4 mJ mol^{-1} K^{-2}, in agreement with the magnetic DFT calculations, and a Debye temperature of 419 K. A λ-like anomaly in the heat capacity near the magnetic transition is suppressed strongly at fields above about 1.5 kOe, when the material is in the ferromagnetic state.

ACKNOWLEDGMENTS

We thank U. K. Rößler for stimulating discussions. Research was supported by the US Department of Energy, Office of Basic Energy Sciences, Materials Sciences and Engineering Division. D.P. acknowledges support from the ORNL LDRD SEED funding project S12-006, "Rare Earth Free Magnets: Compute, Create, Characterize."

[1] S. Mühlbauer, B. Binz, F. Jonietz, C. Pfleiderer, A. Rosch, A. Neubauer, R. Georgii, and P. Böni, Science **323**, 915 (2009).

[2] X. Z. Yu, N. Kanazawa, Y. Onose, K. Kimoto, W. Z. Zhang, S. Ishiwata, Y. Matsui, and Y. Tokura, Nat. Mater. **10**, 106 (2011).

[3] X. Z. Yu, Y. Onose, N. Kanazawa, J. H. Park, J. H. Han, Y. Matsui, N. Nagaosa, and Y. Tokura, Nature (London) **465**, 901 (2010).

[4] W. Münzer, A. Neubauer, T. Adams, S. Mühlbauer, C. Franz, F. Jonietz, R. Georgii, P. Böni, B. Pedersen, M. Schmidt *et al.*, Phys. Rev. B **81**, 041203 (2010).

[5] S. Seki, X. Z. Yu, S. Ishiwata, and Y. Tokura, Science **336**, 198 (2012).

[6] A. N. Bogadnov, M. V. Kudinov, and D. A. Yablonskii, Sov. Phys. Solid State **31**, 1707 (1989).

[7] A. N. Bogdanov, U. K. Rößler, M. Wolf, and K.-H. Müller, Phys. Rev. B **66**, 214410 (2002).

[8] U. K. Rößler, A. N. Bogdanov, and C. Pfleiderer, Nature (London) **442**, 797 (2006).

[9] U. K. Rößler, A. A. Leonov, and A. N. Bogdanov, J. Phys.: Conf. Ser. **303**, 012105 (2011).

[10] K. Kadowaki, K. Okuda, and M. Date, J. Phys. Soc. Jpn. **51**, 2433 (1982).

[11] P. Pedrazzini, H. Wilhelm, D. Jaccard, T. Jarlborg, M. Schmidt, M. Hanfland, L. Akselrud, H. Q. Yuan, U. Schwarz, Y. Grin *et al.*, Phys. Rev. Lett. **98**, 047204 (2007).

[12] Y. Onose, N. Takeshita, C. Terakura, H. Takagi, and Y. Tokura, Phys. Rev. B **72**, 224431 (2005).

[13] P. Bak and M. H. Jensen, J. Phys. C **13**, L881 (1980).

[14] O. Nakanishi, A. Yanase, A. Hasegawa, and M. Kataoka, Solid State Commun. **35**, 995 (1980).

[15] M. Kataoka and O. Nakanishi, J. Phys. Soc. Jpn. **50**, 3888 (1981).

[16] M. Kataoka, O. Nakanishi, A. Yanase, and J. Kanamori, J. Phys. Soc. Jpn. **53**, 3624 (1984).

[17] A. N. Bogdanov and D. A. Yablonskii, Sov. Phys. JETP **68**, 101 (1989).

[18] A. Bogdanov and A. Hubert, J. Magn. Magn. Mater. **138**, 255 (1994).

[19] A. Hamann, D. Lamago, T. Wolf, H. v. Löhneysen, and D. Reznik, Phys. Rev. Lett. **107**, 037207 (2011).

[20] I. Fischer, N. Shah, and A. Rosch, Phys. Rev. B **77**, 024415 (2008).

[21] D. C. Wright and N. D. Mermin, Rev. Mod. Phys. **61**, 385 (1989).

[22] B. Van Laar, J. Solid State Chem. **3**, 154 (1971).

[23] F. Hulliger and E. V. A. Pobitschka, J. Solid State Chem. **1**, 117 (1970).

[24] T. Miyadai, K. Kikuchi, H. Kondo, S. Sakka, K. Arai, and Y. Ishikawa, J. Phys. Soc. Jpn. **52**, 1394 (1983).

[25] S. S. P. Parkin and R. H. Friend, Philos. Mag. B **41**, 95 (1980).

[26] S. S. P. Parkin and R. H. Friend, Physica B + C **99**, 219 (1980).

[27] Y. Kousaka, Y. Nakao, J. Kishine, M. Akita, K. Inoue, and J. Akimitsu, Nucl. Instrum. Methods Phys. Res., Sect. A **600**, 250 (2009).

[28] J. Kishine, K. Inoue, and Y. Yoshida, Prog. Theor. Phys. Suppl. **159**, 82 (2005).

[29] Y. Togawa, T. Koyama, K. Takayanagi, S. Mori, Y. Kousaka, J. Akimitsu, S. Nishihara, K. Inoue, A. S. Ovchinnikov, and J. Kishine, Phys. Rev. Lett. **108**, 107202 (2012).

[30] I. G. Bostrem, J.-I. Kishine, and A. S. Ovchinnikov, Phys. Rev. B **78**, 064425 (2008).

[31] J.-I. Kishine and A. S. Ovchinnikov, Phys. Rev. B **79**, 220405(R) (2009).

[32] J.-I. Kishine, I. V. Proskurin, and A. S. Ovchinnikov, Phys. Rev. Lett. **107**, 017205 (2011).

[33] N. S. Kiselev, A. N. Bogdanov, R. Schäfer, and U. K. Rößler, J. Phys. D **44**, 392001 (2011).

[34] T. Moriya and T. Miyadai, Solid State Commun. **42**, 209 (1982).

[35] A. R. Beal, in *Intercalated Layered Materials*, edited by F. A. Levy (D. Reidel Publishing Company, Dordecht, Holland, 1979), pp. 251–305.

[36] S. S. P. Parkin and R. H. Friend, Philos. Mag. B **41**, 65 (1980).

[37] M. K. Chattopadhyay, P. Arora, and S. B. Roy, J. Phys.: Condens. Matter **21**, 296003 (2009).

[38] L. Ludgren, O. Beckman, V. Attia, S. P. Bhattacheriee, and M. Richardson, Phys. Scr. **1**, 69 (1970).

[39] I. E. Dzyaloshinskii, Sov. Phys. JETP **20**, 665 (1965).

[40] Yu. A. Izyumov and V. M. Laptev, Sov. Phys. JETP **58**, 1267 (1983).

[41] Yu. A. Izyumov, Sov. Phys. Usp. **27**, 845 (1984).

[42] U. K. Rößler (private communication).

[43] N. J. Ghimire, M. A. McGuire, D. S. Parker, B. C. Sales, J.-Q. Yan, V. Keppens, M. Koehler, R. M. Latture, and D. Mandrus, Phys. Rev. B **85**, 224405 (2012), and references therein.

[44] R. A. Steeman, E. Frikkee, S. A. M. Mentink, A. A. Menovsky, G. J. Nieuwenhuys, and J. A. Mydosh, J. Phys.: Condens. Matter **2**, 4059 (1990).

[45] M. Barati, W. R. Datars, T. R. Chien, C. V. Stager, and J. D. Garrett, Phys. Rev. B **48**, 16926 (1993).

[46] T. T. M. Palstra, A. A. Menovsky, and J. A. Mydosh, Phys. Rev. B **33**, 6527 (1986).

[47] C. Kittel, *Introduction to Solid State Physics*, 8th ed. (Wiley, USA, 2005).

[48] M. A. McGuire, A. D. Christianson, A. S. Sefat, B. C. Sales, M. D. Lumsden, R. Jin, E. A. Payzant, D. Mandrus, Y. Luan, V. Keppens *et al.*, Phys. Rev. B **78**, 094517 (2008).

[49] L. J. Li, Y. K. Luo, Q. B. Wang, H. Chen, Z. Ren, Q. Tao, Y. K. Li, X. Lin, M. He, Z. W. Zhu *et al.*, New J. Phys. **11**, 025008 (2009).

[50] J. P. Perdew, K. Burke, and M. Ernzerhof, Phys. Rev. Lett. **77**, 3865 (1996).

[51] P. Blaha, K. Schwarz, G. K. H. Madsen, D. Kvasnicka, and J. Luitz, WIEN2*k, An Augmented Plane Wave + Local Orbitals Program for Calculating Crystal Properties* (Karlheinz Schwarz, Techn. Universitat Wien, Austria, 2001).

[52] I. Dzaloshinsky, J. Phys. Chem. Solids **4**, 241 (1958).

[53] T. Moriya, Phys. Rev. **120**, 91 (1960).

[54] J. F. Janak, Phys. Rev. B **16**, 255 (1977).